Strongly interacting bubbles under an ultrasonic horn

Kyuichi Yasui,* Yasuo Iida,† Toru Tuziuti, Teruyuki Kozuka, and Atsuya Towata
National Institute of Advanced Industrial Science and Technology (AIST), 2266-98 Anagahora, Shimoshidami, Moriyama-ku, Nagoya 463-8560, Japan
(Received 10 August 2007; published 31 January 2008)

Numerical simulations of bubble pulsations have been performed for a system of two bubble clouds in order to study the experimentally observed bubble motion under an ultrasonic horn by high-speed video camera. The comparison between the calculated results and the experimental observation of the bubble pulsation has indicated that the bubble pulsation is strongly influenced by the interaction with surrounding bubbles. The expansion of a bubble during the rarefaction phase of ultrasound is strongly reduced by the bubble-bubble interaction. Some bubbles move toward the horn tip due to the secondary Bjerknes force acting from the bubbles near the horn tip. It has also been shown that the acoustic amplitude in the liquid is strongly reduced by cavitation due to the decrease in acoustic radiation resistance.

DOI: 10.1103/PhysRevE.77.016609 PACS number(s): 43.35.+d, 43.25.+y, 43.30.+m, 78.60.Mq

I. INTRODUCTION

An ultrasonic horn is a device to radiate a strong ultrasonic wave into liquid, gas, and solid [1]. An ultrasonic horn consists of a solid horn connected to an ultrasonic transducer such as piezoelectric ceramics. Since the vibration amplitude of the horn increases as the cross section decreases, the cross section of the horn tip is made much smaller than that of the ultrasonic transducer. While an ultrasonic transducer such as piezoelectric ceramics may be broken at the vibration amplitude much larger than a few micrometers, the vibration amplitude of the horn tip is about an order of magnitude larger than that of the ultrasonic transducer.

When an ultrasonic horn is immersed into the liquid and strong ultrasonic wave is radiated from the horn tip, many bubbles appear near the horn tip, which is called acoustic cavitation [2]. The bubbles repeat expansion and collapse according to the pressure oscillation of an ultrasonic wave [3]. Under some condition, a bubble collapses very violently and the temperature and pressure inside a bubble increase dramatically up to thousands of kelvin and hundreds of atmosphere or more, respectively at the end of the collapse [4–6]. As a result, faint light is emitted from a bubble, which is called sonoluminescence [7,8]. Furthermore, water vapor is dissociated inside the heated bubble and chemical species such as OH radical and H atom are created inside the bubble [9,10]. The chemical products dissolve into the surrounding liquid and react with solutes. Chemical reactions induced or accelerated by ultrasound are called sonochemical reactions [1,11].

An ultrasonic horn has been widely used in liquid not only for sonochemical reactions but also for emulsification, dispersion, cell disruption, extraction, mixing, decreasing the liquid viscosity, etc. [1,11]. In those processes, cavitation may play an important role. Thus, the study on cavitation bubbles under an ultrasonic horn is important to understand those processes and improve their efficiency. In the present study, cavitation bubbles under an ultrasonic horn were observed by high-speed video camera and numerical simulations of bubble pulsations were performed in order to understand the observed bubble motion.

II. EXPERIMENTAL SECTION

An ultrasonic horn (Kouwagiken, Japan) was immersed in liquid water in a rectangular container (87 mm $\times$ 124 mm $\times$ 107 mm). The diameter of the horn tip is 10 mm. The operating frequency of the horn was 29 kHz and the electric power input to the horn was about 5 W or 20 W. The cavitation bubbles were observed by a high-speed video camera (Photoron, FASTCAM-512PCI) and illuminated with LED from the back. The illumination was by the light pulses whose repetition frequency was different from the ultrasonic frequency by 500 Hz. Thus, in 2 ms the phase for the illumination shifted by 2π (one acoustic cycle) relative to the phase of ultrasound. As the frame rate of the video camera is 10 000 fps (0.1 ms for 1 frame), by 20 frames the phase for illumination shifted by 2π. When the video frames were converted into 30 fps for reproduction, one frame was skipped for each two frames. Thus, by ten frames the phase for illumination shifted by 2π. The method of the illumination is essentially the same as reported by Tian *et al.* [12]. The bubble motion recorded in the video frames was analyzed by PC using the software (Himawari, Flow-vec 3) for the analysis of fluid motion with marker particles.

III. EXPERIMENTAL RESULTS

A. 5 W case

Some bubbles moved toward the horn tip. Sometimes bubble streamers were observed [13]. Most of the bubble streamers moved toward the horn tip. Some others moved away from the horn tip at first with a finite velocity component parallel to the surface of the horn tip, but subsequently moved toward the horn tip with a curved trajectory. While the spatial distribution of bubbles near or on the horn tip was inhomogeneous, many bubble streamers moved toward a part of the horn tip where there were many bubbles. These

*k.yasui@aist.go.jp
†y.iida@aist.go.jp

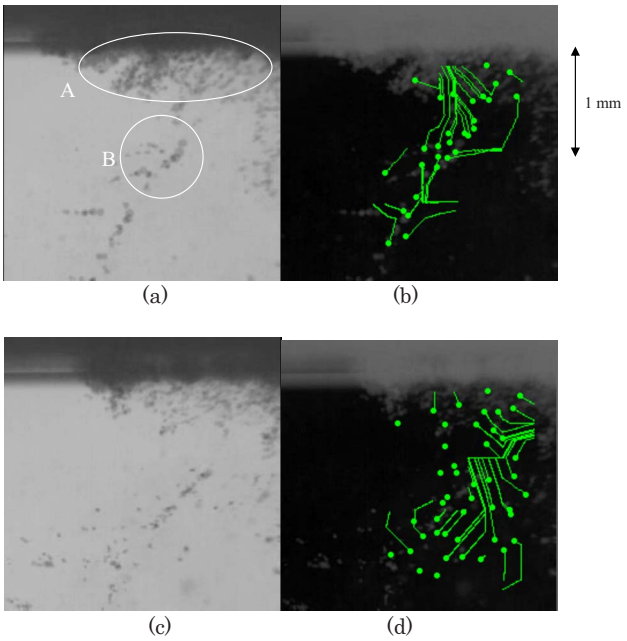

FIG. 1. (Color online) Cavitation bubbles under an ultrasonic horn at 29 kHz and 5 W in frequency and electric power, respectively, observed by a high-speed video camera. The frames (b) and (d) are the results of the analysis of the bubble motion by PC using the software. The small circles are the starting points for the analysis and the curves are the calculated streamlines of bubbles. The frame (b) is the result of the analysis of the bubble motion recorded from the frame (a) to that 2 ms later (not shown here). The frame (d) is the result of the analysis of the bubble motion recorded from the frame (c) [at 4 ms after the frame (a)] to that at 2 ms later (not shown here). For all the analyzed video frames, the phase of the light pulse illuminating the bubbles was at the moment of the bubble expansion. In the frame (a), the bubble clouds *A* and *B* have been marked by circles.

observations are contrasted with the previous reports by Moussatov *et al.* [14,15] that most bubbles moved away from the horn tip.

In Fig. 1, the results of the analysis of the bubble motion by PC using the software have been shown with the video frames. The frame (b) shows the result of the analysis of the bubble motion recorded from the frame (a) to the frame at 2 ms later (not shown here). The phase of the light pulses for the two frames was at the moment of the bubble expansion. The small circles are the starting points for the analysis of the bubble motion and the curves indicate the calculated streamlines of bubbles. It is seen that many bubbles move toward the horn tip where there are many bubbles. On the other hand, some other bubbles move away from the horn tip. The frame (d) shows the result of the analysis of the bubble motion recorded from the frame (c) [at 4 ms after the frame (a)] to the frame at 2 ms later (not shown here). The phase of the light pulses for the two frames was at the moment of the bubble expansion. It is seen that many bubbles move toward the horn tip where there are many bubbles. On the other hand, some other bubbles move away from the horn tip. It is also seen by comparing the frame (b) and (d) that the streamlines of bubbles change dramatically with time in the

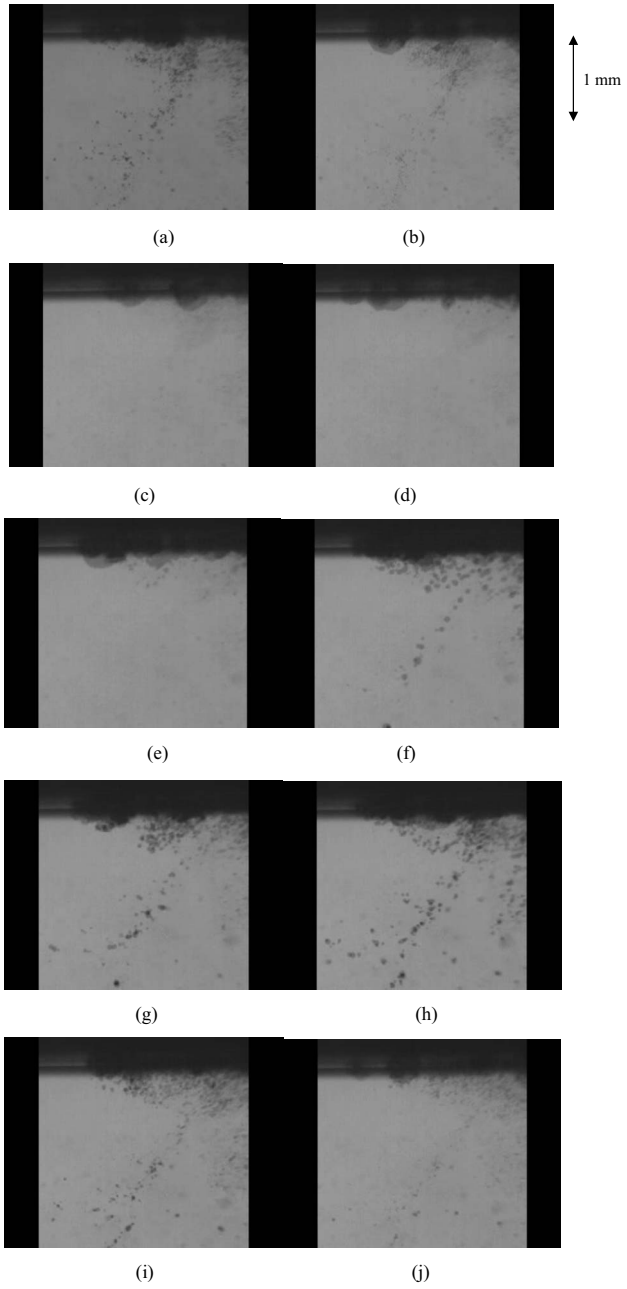

FIG. 2. Ten successive video frames of the bubbles under an ultrasonic horn. In the ten frames, the phase of the light pulse shifted by 2π relative to the phase of ultrasound. The actual time for the ten frames was 2 ms.

time scale of ms corresponding to about 30 acoustic cycles. The velocity of each bubble ranges from about 0.1 m/s to 2 m/s according to the analysis.

Here we shall define the bubble cloud *A* and *B* centered at about 0.3 and 1.1 mm, respectively, below the horn tip as shown in Fig. 1(a). In the bubble cloud *A*, the bubble radius at the bubble expansion ranges from about 15 μm to 50 μm (mostly less than 40 μm). In the bubble cloud *B*, the bubble radius at the bubble expansion ranges from about 15 μm to 50 μm (mostly around 50 μm).

In Fig. 2, the successive ten frames in the video have been shown, which correspond to one acoustic cycle with regard

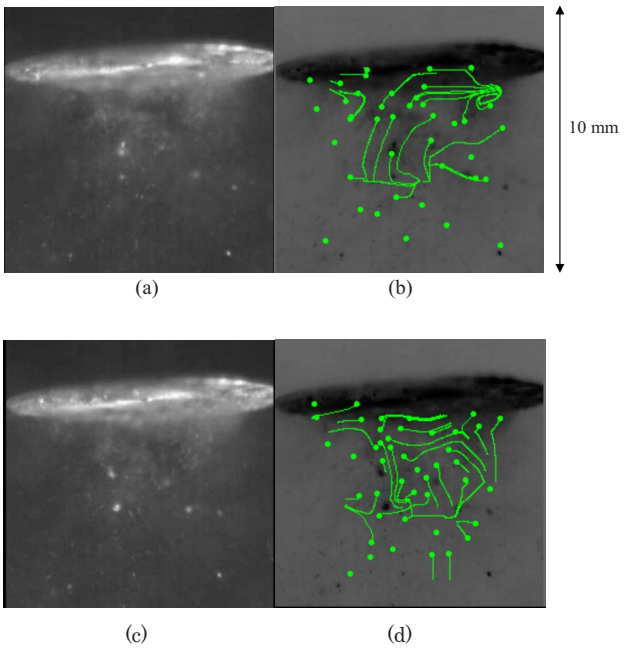

FIG. 3. (Color online) Overview of the horn tip with cavitation bubbles. The illumination was not by the light pulses but by the continuum light. The frame (b) is the result of the analysis of the bubble motion recorded from the frame (a) to that at 0.2 ms later (not shown here) using the software (see the caption of Fig. 1). The frame (d) is the result of the analysis of the bubble motion recorded from the frame (c) [0.6 ms after the frame (a)] to that at 0.2 ms later (not shown here).

to the phase of ultrasound. With regard to the actual time, the ten frames corresponded to 2 ms. From Fig. 2, it is seen that many bubbles pulsate synchronously. Most of the bubbles seen in the frame (a) cannot be seen from the frame (c) to (e) except some large bubbles on the horn tip and few bubbles near the horn tip because the radii of most bubbles are too small (probably less than 10 μm) during the compression phase of ultrasound. Thus, the duration for the small bubble size is $2/5\pi-3/5\pi$ in terms of the phase of ultrasound. In other words, the duration is $7-10$ μs in one acoustic cycle (34.5 μs). In Fig. 2, it is impossible to follow each bubble in the successive frames. It may be due to the frequent coalescence and fragmentation of bubbles.

In Fig. 3, an overview of the horn tip has been shown with cavitation bubbles. The frames (b) and (d) are the results of the analysis of the bubble motion by PC using the software. In Fig. 3, bubbles were illuminated not by the light pulses but by the continuum light. The frame (c) is at 0.6 ms after the frame (a). It is seen that many bubbles near the horn tip (at less than 2 mm from the horn tip) move toward the horn tip, while many other bubbles move away from the horn tip. The bubble motion is rather irregular and changes dramatically with time in the time scale of $0.1-1$ ms corresponding to 3–30 acoustic cycles.

In Fig. 4, the bubble clusters observed have been shown. The phase of the light pulses for the frames (a), (c), and (e) and that for the frames (b) and (d) were at the bubble expansion and at the bubble collapse, respectively. It is seen that bubbles in the clusters do pulsate strongly. Although two

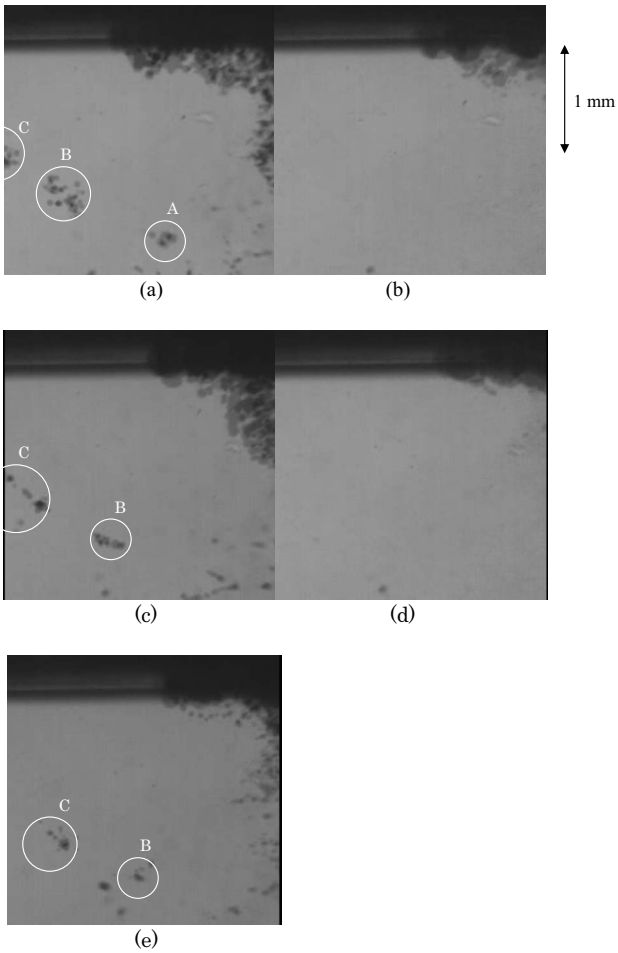

FIG. 4. Bubble clusters observed under an ultrasonic horn. The phase of the light pulses for the frames (a), (c), and (e) and that for the frames (b) and (d) were at the bubble expansion and at the bubble collapse, respectively. The actual time between each frame was 1 ms.

clusters *B* and *C* can be identified in the frames (a), (c), and (e) for totally 4 ms, no individual bubble can be identified even in the two successive frames. It may be due to the frequent coalescence and fragmentation of bubbles in each cluster. A cluster may not be a group of long-lived individual bubbles but a dynamical organization in which bubbles frequently coalesce and fragment.

With regard to the vibration amplitude of the horn tip, it has been experimentally estimated to be 8.5 μm $\pm$ 2.5 μm in peak to peak amplitude from the visual observation.

B. 20 W case

In Fig. 5, the result of the analysis of the bubble motion has been shown. It is seen that many bubbles near the horn tip move toward the horn tip. Many bubbles apart from the horn tip move away from the horn tip. However, the bubble motion is rather irregular.

IV. THEORETICAL MODEL

In the present model for numerical simulations of the pulsation of a bubble, the effect of the bubble-bubble interaction

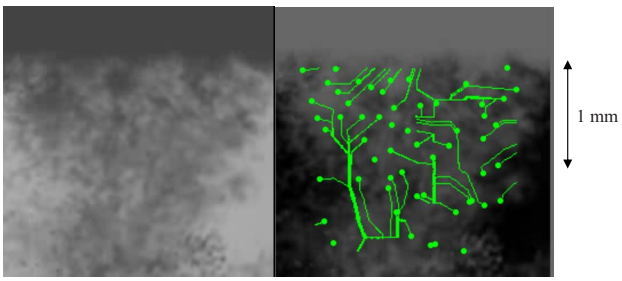

FIG. 5. (Color online) Cavitation bubbles under an ultrasonic horn at 29 kHz and 20 W in frequency and electric power, respectively, observed by the high-speed camera. The frame (b) is the result of the analysis of the bubble motion recorded from the frame (a) to that at 2 ms later using the software (see the caption of Fig. 1). The phase of the light pulse was at the bubble expansion.

has been taken into account through the velocity field of the liquid changed by the pulsations of the surrounding bubbles. The other part of the model is essentially the same with that described in Refs. [16,17].

The following is the description of the model for the effect of the bubble-bubble interaction on the pulsation of a bubble. The velocity field (w) around a pulsating bubble is expressed as Eq. (1) under the incompressible liquid approximation [18].

$$w = \frac{R^2\dot{R}}{r^2}, \tag{1}$$

where R is the radius of a bubble, $\dot{R}=dR/dt$, t is time, and r is the distance from the center of the bubble. At first, we will consider a pair of bubbles following the theoretical method of Mettin *et al.* [18]. Equation (2) has been derived as the equation for the pulsation of a bubble taking into account the effect of the bubble-bubble interaction through Eq. (1). The method for the derivation of Eq. (2) is essentially the same as that for the modified Keller equation described in Refs. [19–21]

$$\begin{aligned}
&\left(1-\frac{\dot{R}}{c_\infty}+\frac{\dot{m}}{c_\infty\rho_{L,i}}\right)R\ddot{R}+\frac{3}{2}\dot{R}^2\left(1-\frac{\dot{R}}{3c_\infty}+\frac{2\dot{m}}{3c_\infty\rho_{L,i}}\right)\\
&\quad=\frac{1}{\rho_{L,\infty}}\left(1+\frac{\dot{R}}{c_\infty}\right)\left[p_B-p_S\left(t+\frac{R}{c_\infty}\right)-p_\infty\right]\\
&\qquad+\frac{\dot{m}R}{\rho_{L,i}}\left(1-\frac{\dot{R}}{c_\infty}+\frac{\dot{m}}{c_\infty\rho_{L,i}}\right)+\frac{\dot{m}}{\rho_{L,i}}\left(\dot{R}+\frac{\dot{m}}{2\rho_{L,i}}\right.\\
&\qquad\left.+\frac{\dot{m}\dot{R}}{2c_\infty\rho_{L,i}}-\frac{R}{\rho_{L,i}}\dot{\rho}_{L,i}-\frac{\dot{m}R}{c_\infty\rho_{L,i}^2}\dot{\rho}_{L,i}\right)\\
&\qquad+\frac{R}{c_\infty\rho_{L,\infty}}\dot{p}_B-\frac{1}{d}\left(2\dot{R}_b^2R_b+R_b^2\ddot{R}_b\right),
\end{aligned} \tag{2}$$

where R is the instantaneous bubble radius, the dot denotes the time derivative (d/dt), t is time, c_∞ is the sound velocity in liquid, $\dot{m}$ is the rate of evaporation of water vapor at the bubble wall (negative value means condensation), $\rho_{L,i}$ is the liquid density at the bubble wall, $\ddot{R}=d^2R/dt^2$, $\rho_{L,\infty}$ is the liquid density far from a bubble, p_B is the liquid pressure at the bubble wall, $p_S(t)$ is the instantaneous pressure of ultrasound at time t, $p_S(t)=-p_a\sin\omega t$, p_a is the pressure amplitude of ultrasound (acoustic amplitude), ω is the angular frequency of ultrasound, p_∞ is the ambient pressure, $\ddot{m}=d\dot{m}/dt$, d is the distance between the two bubbles (the distance from the center of a spherical bubble to that of the other spherical bubble), and R_b is the instantaneous radius of the other bubble. The last term is the influence of the bubble-bubble interaction on the bubble pulsation. The term has been derived from the velocity field changed by the pulsation of the other bubble [Eq. (1)]. Without the last term, Eq. (2) is identical to the modified Keller equation described in Refs. [16,17,19]. It should be noted that the last term is an approximate form neglecting the terms containing $\dot{R}_b/c_\infty$, $R_b\ddot{R}_b/c_\infty\dot{R}_b$, etc. as in Ref. [18]. In order to solve Eq. (2), the corresponding equation for the other bubble should be solved simultaneously in order to calculate R_b.

When the number of bubbles is N, the last term in Eq. (2) should be replaced by the term

$$-\sum_{i=1}^{N-1}\frac{1}{d_i}(2\dot{R}_i^2R_i+R_i^2\ddot{R}_i), \tag{3}$$

where the summation is for the other $N-1$ bubbles, d_i is the distance between the bubble and the bubble i (the distance between the center of the spherical bubble and that of the spherical bubble i), and R_i is the instantaneous radius of the bubble i. In order to calculate the term (3), $N-1$ equations for the pulsation of $N-1$ bubbles should be solved simultaneously to calculate R_i. Thus, the number of equations to be solved simultaneously is N.

When bubbles are spatially homogeneously distributed, the number of equations to be solved can be reduced. If the ambient bubble radius, which is defined as the bubble radius when ultrasound is absent, is the same for all the bubbles and the pressure amplitude of ultrasound is the same for all the bubbles, all the homogeneously distributed bubbles may pulsate exactly in the same manner and the number of equations to be solved is only 1. In this case, the last term of Eq. (2) should be replaced by the term.

$$-\left(\sum_i\frac{1}{d_i}\right)(2\dot{R}^2R+R^2\ddot{R}), \tag{4}$$

where the coefficient of the term is related to the number density of bubbles (n) and the radius ($l_{\max}$) of the bubble cloud in which bubbles are homogeneously distributed as

$$S=\sum_i\frac{1}{d_i}=\int_{l_{\min}}^{l_{\max}}\frac{4\pi r^2n}{r}dr=2\pi n(l_{\max}^2-l_{\min}^2)\approx 2\pi nl_{\max}^2, \tag{5}$$

where the coefficient of the term (4) has been defined as S, $l_{\min}$ is the distance between a bubble and the nearest bubble, and $l_{\max}\gg l_{\min}$ has been assumed. We shall call S the coupling strength because it indicates the strength of coupling (interaction) with surrounding bubbles. It is proportional to

the bubble number density and a square of the radius of the bubble cloud according to Eq. (5). We shall call the system "the homogeneous bubble cloud."

In the present study, we shall consider two homogeneous bubble clouds (A and B in Fig. 1(a)). The last term of Eq. (2) should be replaced by the term (6) for the equation for the pulsation of a bubble in the homogeneous bubble cloud A,

$$-S_A(2\dot{R}_A^2R_A+R_A^2\ddot{R}_A)-S_{BA}(2\dot{R}_B^2R_B+R_B^2\ddot{R}_B), \tag{6}$$

where S_A is the coupling strength in the homogeneous bubble cloud A, R_A is the instantaneous radius of a bubble in the homogeneous bubble cloud A, S_{BA} is the coupling strength of a bubble in the cloud A against all the bubbles in the cloud B, and R_B is the instantaneous radius of a bubble in the homogeneous bubble cloud B. S_{BA} may be estimated by

$$S_{BA}=\sum_{B\to A}\frac{1}{d_i}\approx\frac{N_B}{d_{BA}}, \tag{7}$$

where the summation is for all the bubbles in the cloud B, d_i is the distance between the bubble in the cloud A and a bubble in the cloud B, N_B is the total number of bubbles in the cloud B, and d_{BA} is the distance between the center of the cloud B and that of the cloud A. In order to solve the equation for the pulsation of a bubble in the homogeneous bubble cloud A, the corresponding equation for a bubble in the cloud B should be solved simultaneously in order to calculate R_B.

When the ambient radius of a bubble in the bubble cloud A differs from that of the other bubbles in the cloud A, the last term of Eq. (2) for the bubble should be replaced by the term (6). In order to solve the equation, the equation for the pulsation of the other bubbles in the cloud A and that for a bubble in the cloud B should be solved simultaneously in order to calculate R_A and R_B.

In the present model for the bubble pulsation, the following effects have been taken into account as described in Refs. [16,17]: Nonequilibrium evaporation and condensation of water vapor at the bubble wall and thermal conduction both inside and outside a bubble. In the present numerical simulations, a bubble has been assumed to consist of air and water vapor. The effect of chemical reactions inside a bubble has been neglected.

The effect of the bubble-bubble interaction on the pulsation of a bubble has been studied both theoretically and experimentally by many groups [18,22–34]. However, many of them are on a system of two bubbles [18,22–26] and others are on a single bubble cloud [27–31,34]. Furthermore, in most of the previous studies, the pulsation of bubbles is not by ultrasound but by pressure pulses [22,27–29], hydrodynamic pressure variation [30], or boiling [31]. The numerical studies by Doinikov *et al.* [32] and Payne *et al.* [33] are on weak linear pulsation of bubbles. The numerical study by Luther *et al.* [34] is on the cavitation noise from a multibubble system under ultrasound. In the present theoretical analysis, the effect of the bubble-bubble interaction on the pulsation of a bubble has been studied for a system of two bubble clouds under ultrasound.

Now we will consider three kinds of forces acting on a bubble in an acoustic field [13]. One is the primary Bjerknes force which is the radiation force from an acoustic wave (ultrasound). Another is the secondary Bjerknes force which is the force acting from other bubbles. The other is the buoyant force. Both the primary and secondary Bjerknes forces originate in the pressure difference on the bubble surface. The force instantaneously acting on a bubble is expressed as

$$\vec{F}(t)=-V(t)\vec{\nabla}p(\vec{x},t), \tag{8}$$

where $V(t)$ is the volume of a bubble at time t and $p(\vec{x},t)$ is the instantaneous acoustic pressure at the position of a bubble $(\vec{x})$ at time t. As the instantaneous acoustic pressure oscillates periodically with time, the instantaneously acting force [Eq. (8)] changes with time dramatically including the direction of the force. For the bubble motion, the time averaged force is important,

$$\vec{F}_B=-\langle V(t)\vec{\nabla}p(\vec{x},t)\rangle_T \tag{9}$$

where F_B is the primary or secondary Bjerknes force and $\langle\rangle_T$ means the time averaged value over the acoustic period T. With regard to an ultrasonic wave radiated from an ultrasonic horn, it may be a progressive wave [35]

$$p(\vec{x},t)=-p_a(\vec{x})\sin(\omega t-\vec{k}\cdot\vec{x}), \tag{10}$$

where $p_a(\vec{x})$ is the pressure amplitude of an ultrasonic wave at the position $\vec{x}$, ω is the angular frequency of an ultrasonic wave, and $\vec{k}$ is the wave number vector of an ultrasonic wave. The primary Bjerknes force $(\vec{F}_{B1})$ is calculated by Eq. (9) using Eq. (10) for a progressive wave,

$$\vec{F}_{B1}=\nabla p_a\langle V(t)\sin(\omega t-\vec{k}\cdot\vec{x})\rangle_T-p_a\vec{k}\langle V(t)\cos(\omega t-\vec{k}\cdot\vec{x})\rangle_T. \tag{11}$$

With regard to the secondary Bjerkens force, it is expressed by Eq. (12) and the derivation of Eq. (12) has been described in detail in Ref. [18]

$$\vec{F}_{12}=\frac{\rho}{4\pi d^2}\langle V_2\ddot{V}_1\rangle_T\vec{e}_r, \tag{12}$$

where $\vec{F}_{12}$ is the secondary Bjerknes force acting on bubble 2 from bubble 1, ρ is the liquid density, d is the distance between the two bubbles, V_2 is the volume of bubble 2, V_1 is the volume of bubble 1, $\ddot{V}_1=d^2V_1/dt^2$ and $\vec{e}_r$ is the unit vector directed from bubble 1 to bubble 2. When we consider two bubble clouds A and B, the secondary Bjerknes force acting on a bubble in the cloud A from all the bubbles in the cloud B $(\vec{F}_{BA})$ may be approximately evaluated by

$$\vec{F}_{BA}=\frac{\rho N_B}{4\pi d_{BA}^2}\langle V_A\ddot{V}_B\rangle_T,\vec{e}_{BA}, \tag{13}$$

where N_B is the number of bubbles in cloud B, d_{BA} is the distance between the center of cloud B and that of cloud A, V_A and V_B are the volume of a bubble in cloud A and that in cloud B, respectively, and $\ddot{V}_B=d^2V_B/dt^2$ and $\vec{e}_{BA}$ is the unit

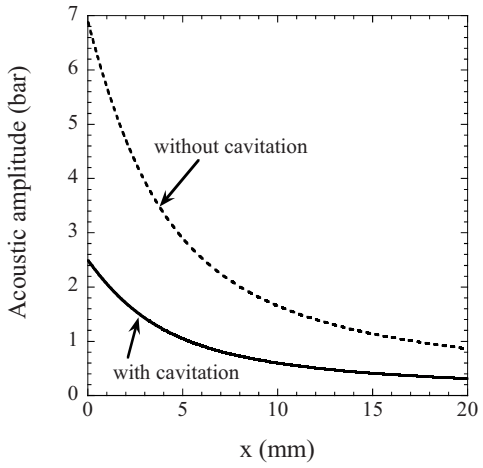

FIG. 6. Calculated acoustic amplitude under an ultrasonic horn as a function of the distance from the horn tip on the symmetry axis. The dotted curve is the calculated result by Eq. (15) using the experimentally measured vibration amplitude of the horn tip as 8.5 μm (peak to peak). The ultrasonic frequency is 29 kHz and the radius of the horn tip is 5 mm. The solid curve is the estimated one by the comparison of the numerical simulation and the experimental observation of the bubble pulsation assuming the spatial variation as Eq. (15).

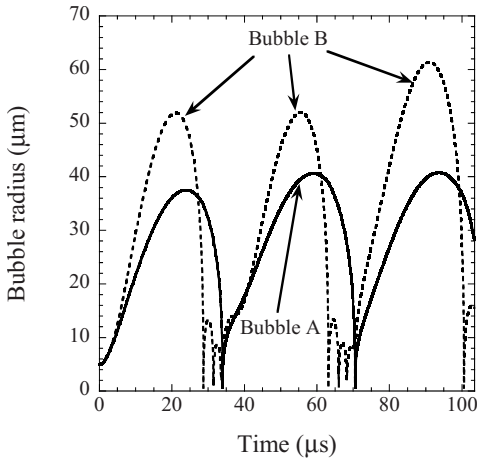

FIG. 7. Calculated bubble radius as a function of time for three acoustic cycles taking into account the interaction of bubbles when the maximum acoustic amplitude at the horn tip is 3 bar at 29 kHz. The solid curve is for a bubble in the cloud A (p_a=2.83 bar) and the dotted one is for a bubble in the cloud B (p_a=2.42 bar). $S_A=1\times10^6$ (m^{-1}), $S_B=1\times10^5$ (m^{-1}), $S_{AB}=4\times10^5$ (m^{-1}), and $S_{BA}=4\times10^4$ (m^{-1}). The ambient bubble radii are both 5 μm.

vector directed from the center of cloud B to that of cloud A. The buoyant force acting on a bubble ($\vec{F}_b$) is expressed as

$$\vec{F}_b = -\rho\vec{g}\left\langle \frac{4}{3}\pi R^3 \right\rangle_T, \tag{14}$$

where ρ is the liquid density, $\vec{g}$ is the gravitational acceleration vector, R is the radius of a bubble, and $\langle\rangle_T$ means the time averaged value over the acoustic period T.

V. NUMERICAL SIMULATIONS AND DISCUSSIONS

The spatial distribution of the pressure amplitude of ultrasound radiated from a circular piston like the horn tip is described on the symmetry axis [36],

$$p_a(x) = \rho c v_0 \left| 2\sin\left(\frac{\pi}{\lambda}(\sqrt{x^2+a^2}-x)\right)\right|, \tag{15}$$

where $p_a(x)$ is the pressure amplitude of ultrasound (acoustic amplitude) at the position x, x is the distance from the circular piston on the symmetry axis, ρ is the liquid density, c is the sound velocity in the liquid, v_0 is the velocity amplitude of the circular piston (the horn tip), λ is the wavelength of ultrasound in the liquid, and a is the radius of the circular piston. When the peak to peak vibration amplitude of the horn tip is 8.5 μm at 29 kHz (for the 5 W case), the velocity amplitude is 0.77 m/s. Then Eq. (15) gives the dotted line in Fig. 6. The maximum acoustic amplitude at the origin is about 7 bar and there is no *near field* because the radius of the horn tip (5 mm) is much smaller than the wavelength of ultrasound in liquid water at 29 kHz (51.7 mm) [36].

Now we will show that the actual acoustic amplitude near the horn tip in the experiment is far less than that (7 bar) predicted by Eq. (15). In the following numerical simulations, we will consider two bubble clouds. The bubble cloud A is centered at about 0.3 mm from the horn tip and the bubble cloud B is centered at about 1.1 mm from the horn tip [Fig. 1(a)]. The number density of bubbles in the cloud A is much larger than that of the cloud B as seen in Fig. 1(a). In Fig. 7, the result of the numerical simulation of the bubble pulsation has been shown when the maximum acoustic amplitude at the horn tip is 3 bar. The acoustic amplitude in the bubble cloud A and that in the bubble cloud B have been assumed as 2.83 bar and 2.42 bar, respectively, assuming the spatial variation as Eq. (15). According to Fig. 1(a), the typical maximum radius of a bubble in the cloud A is about 40 μm and that in the cloud B is about 50 μm. In order to reproduce the maximum radii, the coupling strength of the cloud A and that of the cloud B should be $S_A=1\times10^6$(m^{-1}) and $S_B=1\times10^5$(m^{-1}), respectively, when the ambient radius of a typical active bubble is assumed as 5 μm as experimentally reported in Refs. [18,37]. In this case, the coupling strength between the two clouds are $S_{AB}=4\times10^5$(m^{-1}) and $S_{BA}=4\times10^4$(m^{-1}) according to Eqs. (5) and (7) assuming $l_{\max}$=0.5 mm for both the cloud A and the cloud B. From Fig. 7, the duration for the smaller bubble radius than about 10 μm is about 1 μs at the bubble collapse for a bubble in the cloud A (at 33.8–35.1 μs and 70.4–71.7 μs in Fig. 7). It apparently contradicts with the experimental observation shown in Fig. 2 that the duration is 7–10 μs. According to numerical simulations, such long duration for the small bubble size has never been obtained at higher acoustic amplitude than 3 bar at the horn tip. Thus, it is concluded that the maximum acoustic amplitude at the horn tip is less than 3 bar.

When the maximum acoustic amplitude at the horn tip is 2.5 bar, the long duration for the small bubble size has been obtained by the numerical simulation (Fig. 8). The acoustic amplitude at the cloud A and that at the cloud B have been

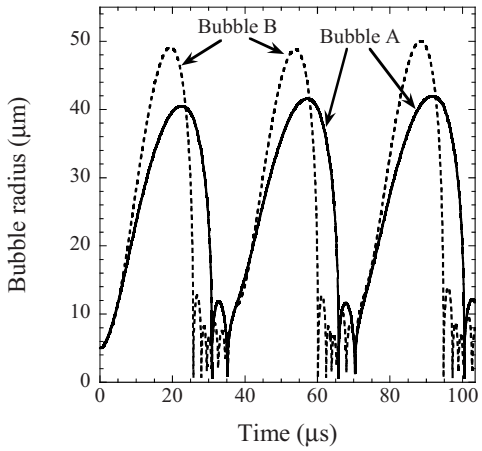

FIG. 8. Calculated bubble radius as a function of time for three acoustic cycles taking into account the interaction of bubbles when the maximum acoustic amplitude at the horn tip is 2.5 bar at 29 kHz. The solid curve is for a bubble in the cloud A (p_a =2.36 bar) and the dotted one is for a bubble in the cloud B (p_a =2.02 bar). $S_A=5\times10^5$ (m^{-1}), $S_B=5\times10^4$ (m^{-1}), $S_{AB}=2\times10^5$ (m^{-1}), and $S_{BA}=2\times10^4$ (m^{-1}). The ambient bubble radii are both 5 μm.

assumed as 2.36 bar and 2.02 bar, respectively, assuming the spatial variation as Eq. (15). In this case, the coupling strength should be $S_A=5\times10^5$ (m^{-1}) and $S_B=5\times10^4$ (m^{-1}) in order to reproduce the typical maximum radii of bubbles in Fig. 1(a). Then the total number of bubbles in the cloud A and that in the cloud B are 170 and 17, respectively, according to Eq. (5) assuming $l_{\max}=0.5$ mm for the both clouds. In the video image of Fig. 1(a), the number of bubbles in the cloud A and that in the cloud B have been directly counted as about 200 and 20, respectively. Thus the number of bubbles resulted in the present analysis is consistent with the experimental observation. Then, the coupling strength between the two clouds is $S_{AB}=2\times10^5$ (m^{-1}) and $S_{BA}=2\times10^4$ (m^{-1}). From Fig. 8, the duration for the small bubble size at the bubble collapse is about 6 μs for a bubble in the cloud A (at 30.8–36.8 μs and 65.7–72.0 μs in Fig. 8) and about 10 μs for a bubble in the cloud B (at 25.7–36.8 μs and 62.0–71.5 μs in Fig. 8), which is almost consistent with the experimental observation (Fig. 2). It should be noted here that the coupling constants and the number of bubbles estimated in the present theoretical analysis may have some errors due to the assumption of a single bubble size and spatially homogeneous distribution of bubbles.

When the maximum acoustic amplitude at the horn tip is less than 2 bar, the calculated maximum radius of a bubble in the cloud A and that in the cloud B are both smaller than the typical ones experimentally observed if we assume the number of bubbles in the cloud A and B is about 200 and 20, respectively. Thus it is concluded that the maximum acoustic amplitude at the horn tip is larger than 2 bar. It means that the actual acoustic amplitude at the horn tip in the experiment is about 2.5 bar (above 2 bar and below 3 bar).

Why is the actual acoustic amplitude at the horn tip (about 2.5 bar) much smaller than the value predicted by the vibration amplitude of the horn tip using Eq. (15) (7 bar)? According to Ref. [38], the acoustic radiation resistance drops by cavitation to about 1/3 of the value without cavitation. The acoustic radiation resistance is the real part of the acoustic radiation impedance (Z) [39]

$$Z=\frac{p_{\rm rad}}{U}, \tag{16}$$

where $p_{\rm rad}$ is the pressure amplitude of ultrasound radiated by an ultrasonic transducer (or the horn tip) and U is the amplitude of the volume velocity of an ultrasonic transducer (or the horn tip) which is defined as the surface integral of the velocity amplitude over the radiating surface. Thus, when the acoustic radiation resistance drops to about 1/3, the acoustic amplitude at the radiating surface drops to about 1/3 if the vibration amplitude of the radiating surface is the same. It is consistent with the drop of the acoustic amplitude at the horn tip from 7 bar without cavitation [estimated by Eq. (15)] to 2.5 bar with cavitation (about 1/3 of 7 bar). Thus it is concluded that the actual acoustic amplitude in the liquid is much smaller than that estimated by Eq. (15) due to the drop of the acoustic radiation resistance by cavitation (Fig. 6). It should be noted that the actual acoustic amplitude may vary with time due to the variation of the bubble number density on the horn tip.

Next we will discuss the reason for the bubble motion toward the horn tip observed in Figs. 1 and 3. The results of the numerical simulation on the forces acting on a bubble have been summarized as follows.

A. The forces acting on a bubble in the cloud A

(1) The primary Bjerknes force:

$$\nabla p_a\langle V_A(t)\sin(\omega t-\vec{k}\cdot\vec{x})\rangle_T=2.19\times10^{-6}(N)$$

away from the horn tip,

$$-p_a\vec{k}\langle V_A(t)\cos(\omega t-\vec{k}\cdot\vec{x})\rangle_T=1.67\times10^{-6}(N)$$

away from the horn tip.

(2) The secondary Bjerknes force from all the bubbles in the cloud B:

$$-\frac{\rho}{4\pi d_{BA}^2}\langle V_A\ddot{V}_B\rangle N_B=8.55\times10^{-5}(N)$$

away from the horn tip.

(3) The buoyant force:

$$-\rho g\left\langle\frac{4}{3}\pi R_A^3\right\rangle_T=-1.24\times10^{-9}(N)\quad\text{toward the horn tip.}$$

(4) The sum of the forces:

$$8.94\times10^{-5}(N)\quad\text{away from the horn tip.}$$

B. The forces acting on a bubble in the cloud B

(1) The primary Bjerknes force:

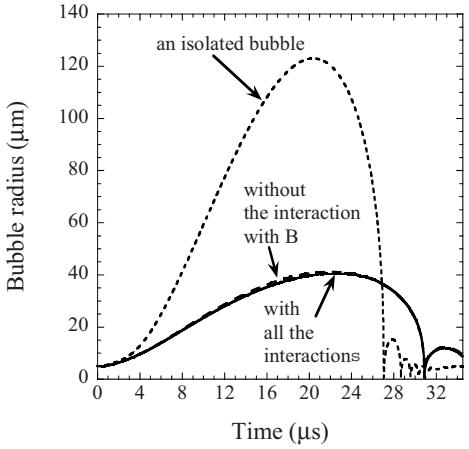

FIG. 9. Calculated radius of a bubble in the cloud *A* as a function of time for one acoustic cycle at 29 kHz and 2.36 bar in frequency and pressure amplitude of ultrasound, respectively. The ambient bubble radius is 5 μm. The dotted curve is the calculated result neglecting all the interactions with other bubbles (an isolated bubble). The dashed one is the calculated result neglecting only the interaction with the bubbles in the cloud *B*. The solid one is the calculated result taking into account all the interactions with surrounding bubbles.

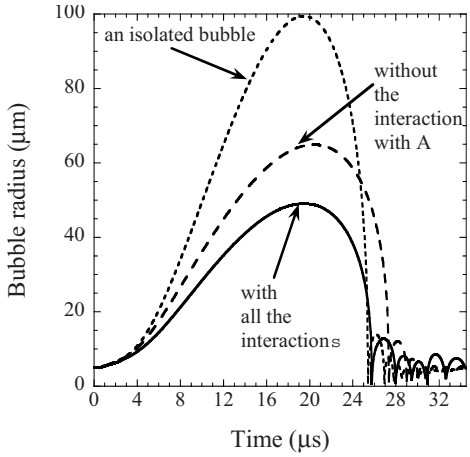

FIG. 10. Calculated radius of a bubble in the cloud *B* as a function of time for one acoustic cycle at 29 kHz and 2.02 bar in frequency and pressure amplitude of ultrasound, respectively. The ambient bubble radius is 5 μm. The dotted curve is the calculated result neglecting all the interactions with other bubbles (an isolated bubble). The dashed one is the calculated result neglecting only the interaction with the bubbles in the cloud *A*. The solid one is the calculated result taking into account all the interactions with surrounding bubbles.

$$\nabla p_a \langle V_B(t) \sin(\omega t - \vec{k}\cdot\vec{x})\rangle_T = 6.87 \times 10^{-7}(N)$$

away from the horn tip.

$$-p_a \vec{k} \langle V_B(t) \cos(\omega t - \vec{k}\cdot\vec{x})\rangle_T = 2.87 \times 10^{-6}(N)$$

away from the horn tip.

(2) The secondary Bjerknes force from all the bubbles in the cloud *A*:

$$\frac{\rho}{4\pi d_{AB}^2} \langle V_B \ddot{V}_A \rangle N_A = -8.55 \times 10^{-4}(N) \quad \text{toward the horn tip.}$$

(3) The buoyant force:

$$-\rho g \left\langle \frac{4}{3}\pi R_B^3 \right\rangle_T = -1.56 \times 10^{-9}(N) \quad \text{toward the horn tip.}$$

(4) The sum of the forces:

$$-8.51 \times 10^{-4}(N) \quad \text{toward the horn tip.}$$

From the above results, it is concluded that some bubbles in the cloud *B* move toward the horn tip due to the secondary Bjerknes force from the bubbles in the cloud *A* near the horn tip. It is consistent with the experimental observation shown in Fig. 1. It should be noted that the actual bubble motion is rather irregular, as seen in Figs. 1 and 3, because the secondary Bjerknes force between bubbles in the same cloud is also important and it strongly depends on the spatial distribution of the surrounding bubbles which vary with time.

Next we will discuss the influence of the bubble-bubble interaction on the pulsation of a bubble. In Fig. 9, the comparison of the radius-time curves has been shown for a bubble in the cloud *A* for the following three cases. One is for the case neglecting all the interactions with the other bubbles. Such a bubble is called an isolated one. Another is for the case neglecting only the interaction with the bubbles in the cloud *B*. The other is for the case taking into account all the interactions with the other bubbles. It is seen from Fig. 9 that the pulsation of a bubble is strongly influenced by the bubble-bubble interaction. The expansion of a bubble is strongly reduced by the interaction with the surrounding bubbles. In this case, however, the influence of the cloud *B* is negligible on the pulsation of a bubble in the cloud *A*.

In Fig. 10, the comparison of the radius-time curves has been shown for a bubble in the cloud *B* for the three cases similar to Fig. 9. Again, it is seen that the pulsation of a bubble is strongly influenced by the bubble-bubble interaction. As in the case of Fig. 9, the expansion of a bubble is strongly reduced by the interaction with the surrounding bubbles. In this case, the cloud *A* influences considerably the pulsation of a bubble in the cloud *B*.

In Fig. 11, the results of the numerical simulations have been shown for a bubble of different ambient bubble radius from that of the other bubbles in the cloud *A*. The results for an isolated bubble have also been shown. The horizontal axis is the ambient radius of a bubble in logarithmic scale and the vertical axis is the maximum radius of a bubble at the bubble expansion. Again, it is seen that the expansion of a bubble is strongly reduced by the interaction with surrounding bubbles. The range of the maximum bubble radius of 15–50 μm observed experimentally in Fig. 1 corresponds to the range of ambient bubble radius of 3–7 μm for interacting bubbles. It is consistent with the experimentally reported typical ambient bubble radii at around 30 kHz [18,37]. It is also seen from the result for an isolated bubble in Fig. 11 that, without taking into account the effect of the bubble-bubble interaction, the experimentally observed maximum radii of bubbles in Fig. 1 can never been explained. Thus it is

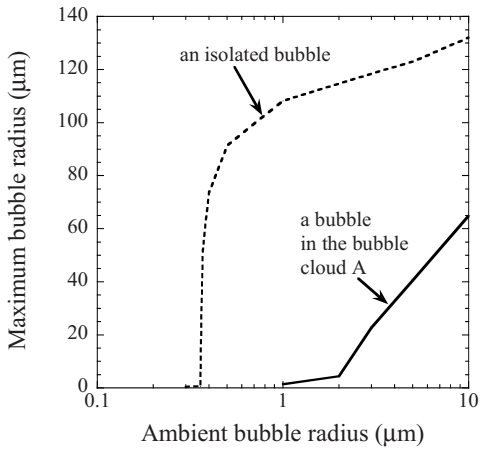

FIG. 11. Calculated maximum bubble radius as a function of the ambient bubble radius with the logarithmic horizontal axis when the frequency and pressure amplitude of ultrasound are 29 kHz and 2.36 bar, respectively. The dotted curve is the calculated result neglecting all the interactions with surrounding bubbles (an isolated bubble). The solid curve is the calculated result for a bubble in the cloud *A* taking into account all the interactions with surrounding bubbles. The ambient radii of the other bubbles are 5 μm.

concluded that the pulsation of a bubble under an ultrasonic horn is strongly influenced by the bubble-bubble interaction.

VI. CONCLUSIONS

The theoretical model of the pulsation of a bubble has been developed for a system of two bubble clouds taking into account the bubble-bubble interaction. Numerical simulations of the bubble pulsation have been performed in order to study the motion of bubbles under an ultrasonic horn experimentally observed by a high-speed video camera. The comparison between the calculated results and the experimental observation of the bubble pulsation has indicated that the bubble pulsation is strongly influenced by the bubble-bubble interaction. The expansion of a bubble during the rarefaction phase of ultrasound is strongly reduced by the interaction with surrounding bubbles. Some bubbles move toward the horn tip due to the secondary Bjerknes force acting from the bubbles near the horn tip. It has also been shown that the acoustic amplitude is strongly reduced by cavitation due to the decrease in the acoustic radiation resistance.

[1] T. J. Mason, *Sonochemistry* (Oxford University Press, Oxford, 1999).
[2] F. R. Young, *Cavitation* (Imperial College, London, 1999).
[3] W. Lauterborn, T. Kurz, R. Mettin, and C. D. Ohl, Adv. Chem. Phys. **110**, 295 (1999).
[4] K. Yasui, J. Acoust. Soc. Am. **112**, 1405 (2002).
[5] W. B. McNamara III, Y. T. Didenko, and K. S. Suslick, Nature (London) **401**, 772 (1999).
[6] W. B. McNamara III, Y. T. Didenko, and K. S. Suslick, J. Phys. Chem. B **107**, 7303 (2003).
[7] F. R. Young, *Sonoluminescence* (CRC Press, Boca Raton, 2005).
[8] K. Yasui, T. Tuziuti, M. Sivakumar, and Y. Iida, Appl. Spectrosc. Rev. **39**, 399 (2004).
[9] A. Henglein, in *Advances in Sonochemistry*, edited by T. J. Mason (JAI Press, London, 1993), Vol. 3, p. 17.
[10] P. Riesz and T. Kondo, Free Radic Biol. Med. **13**, 247 (1992).
[11] *Advances in Sonochemistry*, edited by T. J. Mason (JAI, London/Elsevier, Amsterdam, 1990-2001), Vols. 1–6.
[12] Y. Tian, J. A. Ketterling, and R. E. Apfel, J. Acoust. Soc. Am. **100**, 3976 (1996).
[13] R. Mettin, *in Bubble and Particle Dynamics in Acoustic Fields: Modern Trends and Applications*, edited by A. A. Doinikov (Research Signpost, Kerala, India, 2005), p. 1.
[14] A. Moussatov, C. Granger, and B. Dubus, Ultrason. Sonochem. **10**, 191 (2003).
[15] A. Moussatov, R. Mettin, C. Granger, T. Tervo, B. Dubus, and W. Lauterborn, in Proceedings of the World Congress on Ultrasonics (WCU2003) (Société Française d'Acoustique, Paris, 2003), p. 955.
[16] K. Yasui, T. Tuziuti, M. Sivakumar, and Y. Iida, J. Chem. Phys. **122**, 224706 (2005).
[17] K. Yasui, Phys. Rev. E **56**, 6750 (1997).
[18] R. Mettin, I. Akhatov, U. Parlitz, C. D. Ohl, and W. Lauterborn, Phys. Rev. E **56**, 2924 (1997).
[19] K. Yasui, J. Phys. Soc. Jpn. **65**, 2830 (1996).
[20] J. B. Keller and M. Miksis, J. Acoust. Soc. Am. **68**, 628 (1980).
[21] A. Prosperetti and A. Lezzi, J. Fluid Mech. **168**, 457 (1986).
[22] M. Ida, T. Naoe, and M. Futakawa, Phys. Rev. E **75**, 046304 (2007).
[23] N. A. Pelekasis, A. Gaki, A. Doinikov, and J. A. Tsamopoulos, J. Fluid Mech. **500**, 313 (2004).
[24] A. Pearson, E. Cox, J. R. Blake, and S. R. Otto, Eng. Anal. Boundary Elem. **28**, 295 (2004).
[25] A. Harkin, T. J. Kaper, and A. Nadim, J. Fluid Mech. **445**, 377 (2001).
[26] S. Fujikawa and H. Takahira, Acustica **61**, 188 (1986).
[27] M. Arora, C. D. Ohl, and D. Lohse, J. Acoust. Soc. Am. **121**, 3432 (2007).
[28] N. Bremond, M. Arora, C. D. Ohl, and D. Lohse, Phys. Rev. Lett. **96**, 224501 (2006).
[29] N. Bremond, M. Arora, S. M. Dammer, and D. Lohse, Phys. Fluids **18**, 121505 (2006).
[30] A. Kubota, H. Kato, and H. Yamaguchi, J. Fluid Mech. **240**, 59 (1992).
[31] G. L. Chahine and H. L. Liu, J. Fluid Mech. **156**, 257 (1985).
[32] A. A. Doinikov, R. Manasseh, and A. Ooi, J. Acoust. Soc. Am. **117**, 47 (2005).
[33] E. M. B. Payne, S. J. Illesinghe, A. Ooi, and R. Manasseh, J. Acoust. Soc. Am. **118**, 2841 (2005).
[34] S. Luther, M. Sushchik, U. Parlitz, I. Akhatov, and W. Lauterborn, in *Nonlinear Acoustics at the Turn of the Millennium: ISNA 15*, edited by W. Lauterborn and T. Kurz, AIP Conf.

Proc. No. 524 (AIP, New York, 2000), p. 355.
[35] P. Koch, R. Mettin, and W. Lauterborn, in Proceedings of CFA/DAGA'04, edited by D. Casseraeu (Deutsche Gesellschaft Akustik e.V. (DEGA), Strasbourg, 2004), p. 919.
[36] L. E. Kinsler, A. R. Frey, A. B. Coppens, and J. V. Sanders, *Fundamentals of Acoustics* (Wiley, New York, 1982).
[37] K. R. Weninger, C. G. Camara, and S. J. Putterman, Phys. Rev. E **63**, 016310 (2001).
[38] Y. Kikuchi and H. Shimizu, J. Acoust. Soc. Am. **31**, 1385 (1959).
[39] P. M. Morse and K. U. Ingard, *Theoretical Acoustics* (Princeton University Press, Princeton, NJ, 1968).